Supplementary material for LHCb-PAPER-2021-021

An illustration of the LHCb measurements of Ω_c^0 and Ξ_c^0 lifetimes and the previous world average is shown in Fig. 1, and the fit projections to the invariant mass and $\log_{10}\chi^2_{\rm IP}$ distributions in different decay-time intervals and data-taking periods are shown in Fig. 2–25.

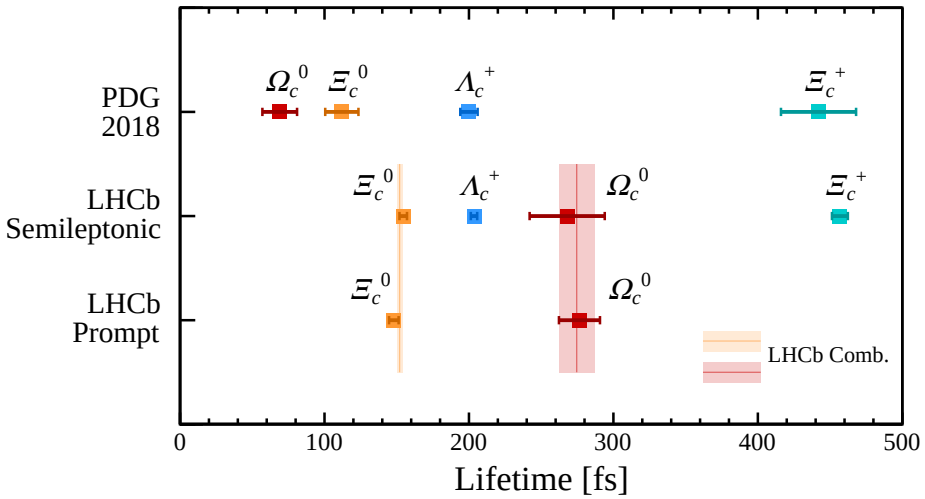

Figure 1: Illustration of the LHCb measurements of the Ω_c^0 and Ξ_c^0 lifetimes obtained from semileptonic beauty-hadron decays [1, 2] and prompt signals, and the previous 2018 world average [3]. The combined LHCb results are shown in coloured bands.

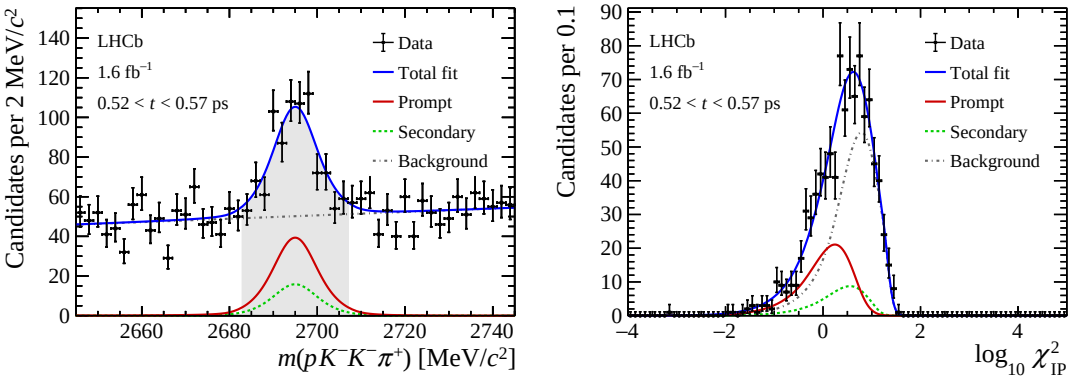

Figure 2: Distributions of (left) invariant mass and (right) $\log_{10}\chi^2_{\rm IP}$ in the reduced mass region of $[2683, 2707]\,\text{MeV}/c^2$ for the Ω_c^0 data sample collected in 2016 in the decay-time interval of $[0.52, 0.57]\,\text{ps}$, along with the fit results. The contributions of the signal, the secondary decays, and the combinatorial background are shown in red (solid), green (dashed), and gray (dash-dotted), respectively.

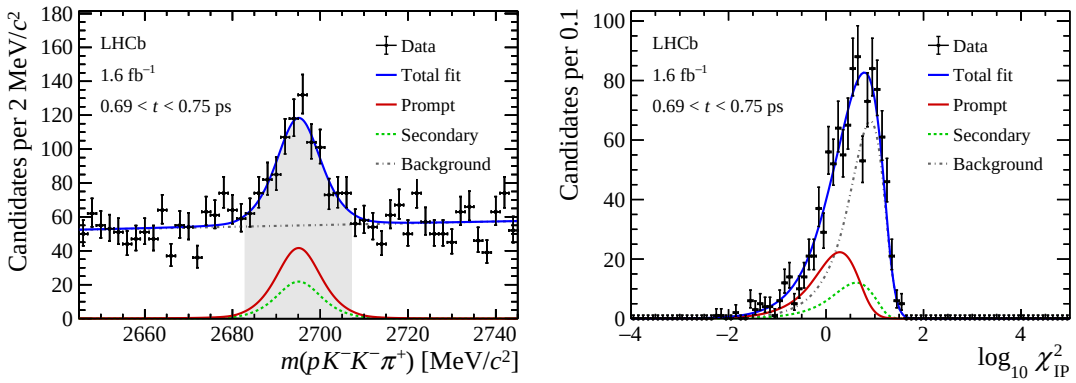

Figure 3: Distributions of (left) invariant mass and (right) $\log_{10}\chi^2_{\rm IP}$ in the reduced mass region of $[2683, 2707]\,\mathrm{MeV}/c^2$ for the Ω_c^0 data sample collected in 2016 in the decay-time interval of $[0.69, 0.75]\,\mathrm{ps}$, along with the fit results. The contributions of the signal, the secondary decays, and the combinatorial background are shown in red (solid), green (dashed), and gray (dash-dotted), respectively.

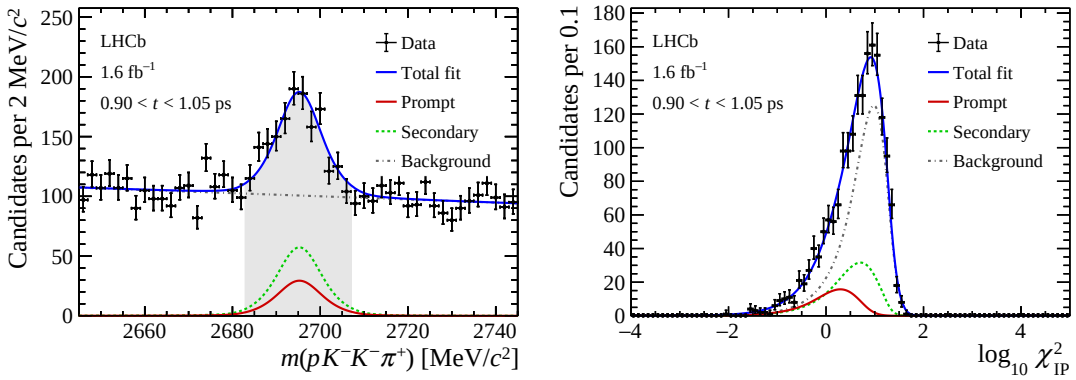

Figure 4: Distributions of (left) invariant mass and (right) $\log_{10}\chi^2_{\rm IP}$ in the reduced mass region of $[2683, 2707]\,\mathrm{MeV}/c^2$ for the Ω_c^0 data sample collected in 2016 in the decay-time interval of $[0.90, 1.05]\,\mathrm{ps}$, along with the fit results. The contributions of the signal, the secondary decays, and the combinatorial background are shown in red (solid), green (dashed), and gray (dash-dotted), respectively.

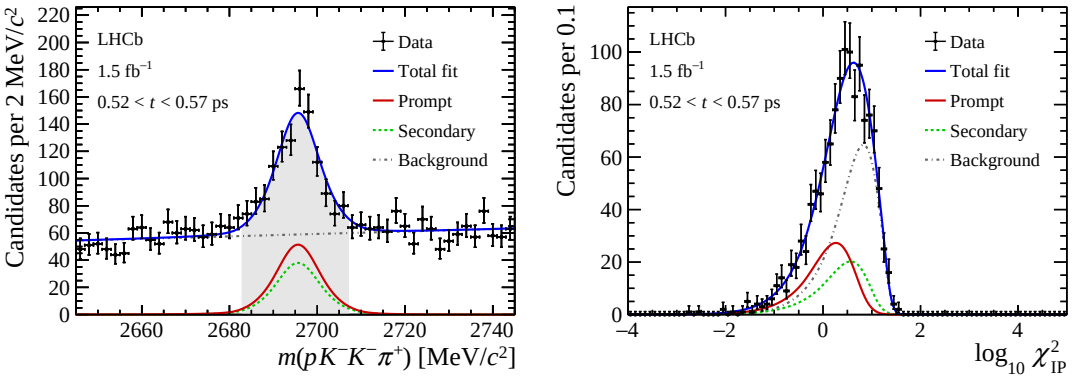

Figure 5: Distributions of (left) invariant mass and (right) $\log_{10}\chi^2_{\rm IP}$ in the reduced mass region of $[2683, 2707]\,\text{MeV}/c^2$ for the Ω_c^0 data sample collected in 2017 in the decay-time interval of $[0.52, 0.57]\,\text{ps}$, along with the fit results. The contributions of the signal, the secondary decays, and the combinatorial background are shown in red (solid), green (dashed), and gray (dash-dotted), respectively.

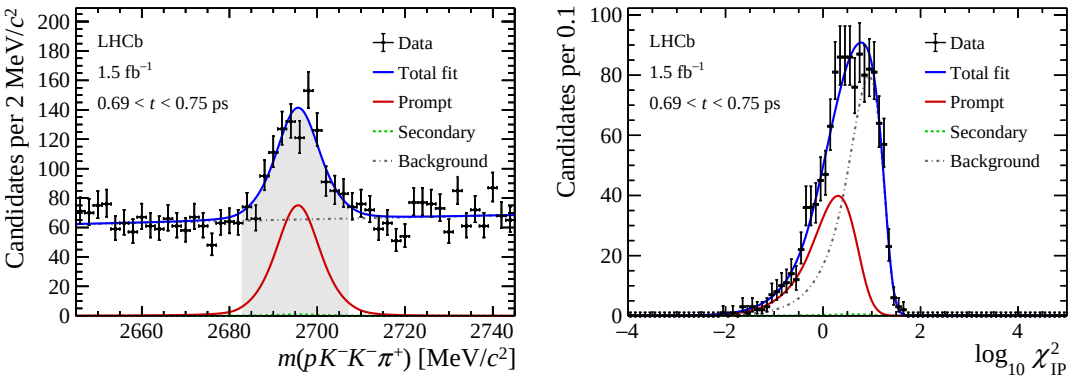

Figure 6: Distributions of (left) invariant mass and (right) $\log_{10}\chi^2_{\rm IP}$ in the reduced mass region of $[2683, 2707]\,\text{MeV}/c^2$ for the Ω_c^0 data sample collected in 2017 in the decay-time interval of $[0.69, 0.75]\,\text{ps}$, along with the fit results. The contributions of the signal, the secondary decays, and the combinatorial background are shown in red (solid), green (dashed), and gray (dash-dotted), respectively.

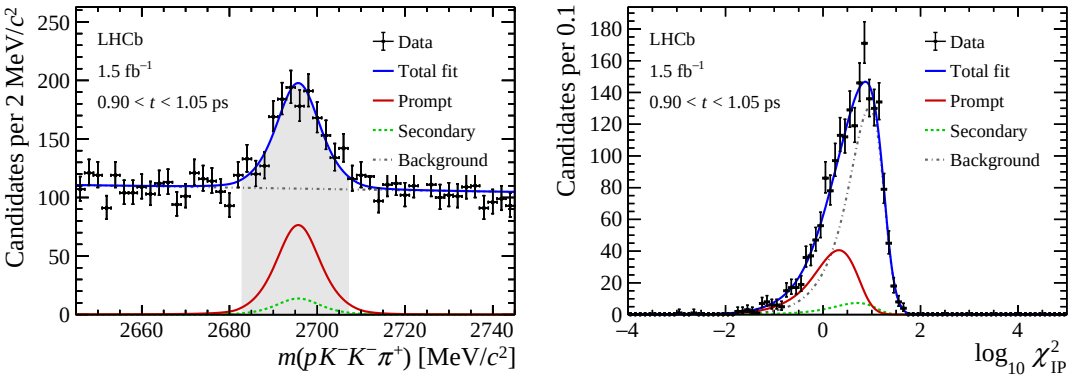

Figure 7: Distributions of (left) invariant mass and (right) $\log_{10}\chi^2_{\rm IP}$ in the reduced mass region of $[2683, 2707]\,\text{MeV}/c^2$ for the Ω_c^0 data sample collected in 2017 in the decay-time interval of $[0.90, 1.05]\,\text{ps}$, along with the fit results. The contributions of the signal, the secondary decays, and the combinatorial background are shown in red (solid), green (dashed), and gray (dash-dotted), respectively.

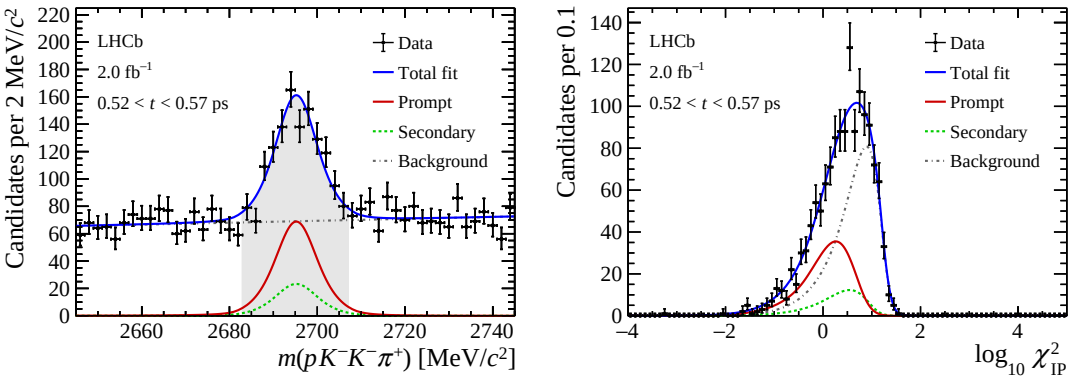

Figure 8: Distributions of (left) invariant mass and (right) $\log_{10}\chi^2_{\rm IP}$ in the reduced mass region of $[2683, 2707]\,\text{MeV}/c^2$ for the Ω_c^0 data sample collected in 2018 in the decay-time interval of $[0.52, 0.57]\,\text{ps}$, along with the fit results. The contributions of the signal, the secondary decays, and the combinatorial background are shown in red (solid), green (dashed), and gray (dash-dotted), respectively.

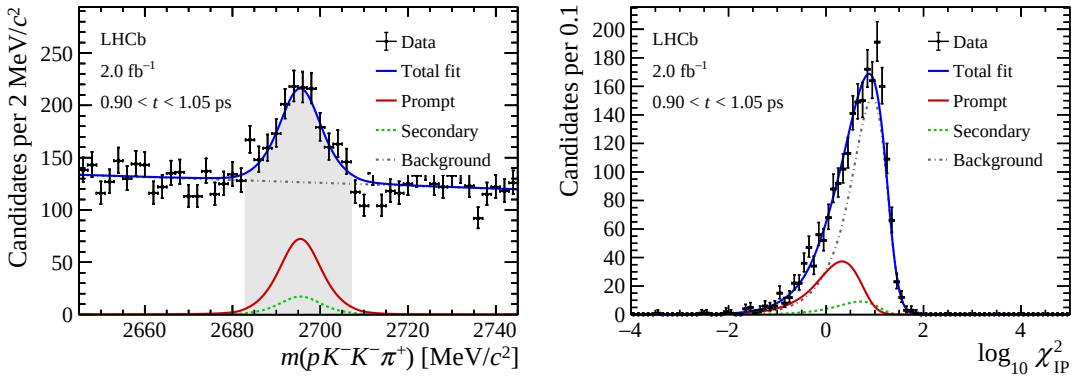

Figure 9: Distributions of (left) invariant mass and (right) $\log_{10}\chi^2_{\rm IP}$ in the reduced mass region of $[2683, 2707]\,\text{MeV}/c^2$ for the Ω_c^0 data sample collected in 2018 in the decay-time interval of $[0.90, 1.05]\,\text{ps}$, along with the fit results. The contributions of the signal, the secondary decays, and the combinatorial background are shown in red (solid), green (dashed), and gray (dash-dotted), respectively.

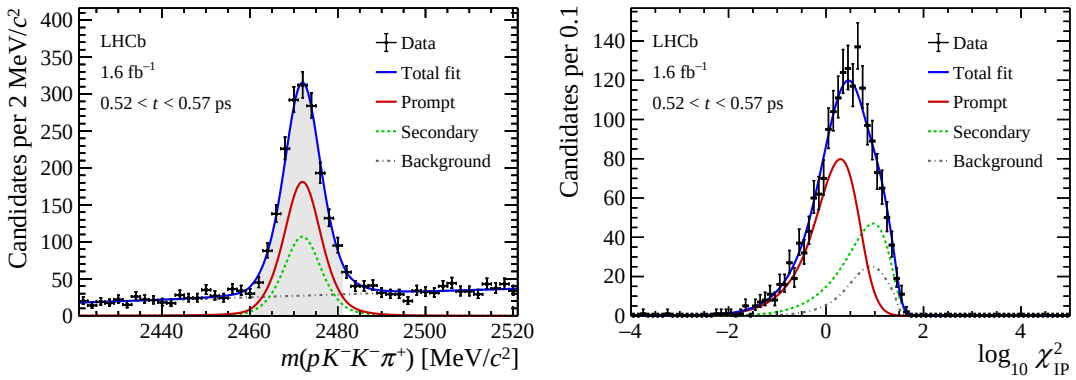

Figure 10: Distributions of (left) invariant mass and (right) $\log_{10}\chi^2_{\rm IP}$ in the reduced mass region of $[2461, 2481]\,\text{MeV}/c^2$ for the Ξ_c^0 data sample collected in 2016 in the decay-time interval of $[0.52, 0.57]\,\text{ps}$, along with the fit results. The contributions of the signal, the secondary decays, and the combinatorial background are shown in red (solid), green (dashed), and gray (dash-dotted), respectively.

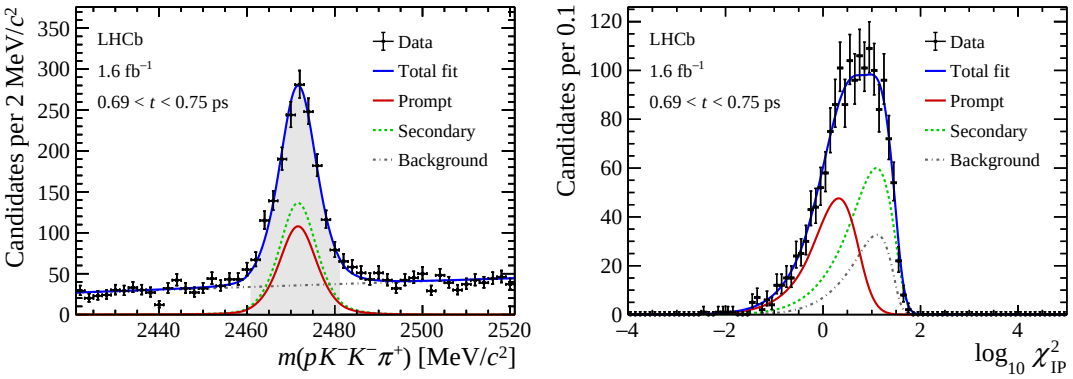

Figure 11: Distributions of (left) invariant mass and (right) $\log_{10}\chi^2_{\rm IP}$ in the reduced mass region of $[2461, 2481]\,\mathrm{MeV}/c^2$ for the Ξ_c^0 data sample collected in 2016 in the decay-time interval of $[0.69, 0.75]\,\mathrm{ps}$, along with the fit results. The contributions of the signal, the secondary decays, and the combinatorial background are shown in red (solid), green (dashed), and gray (dash-dotted), respectively.

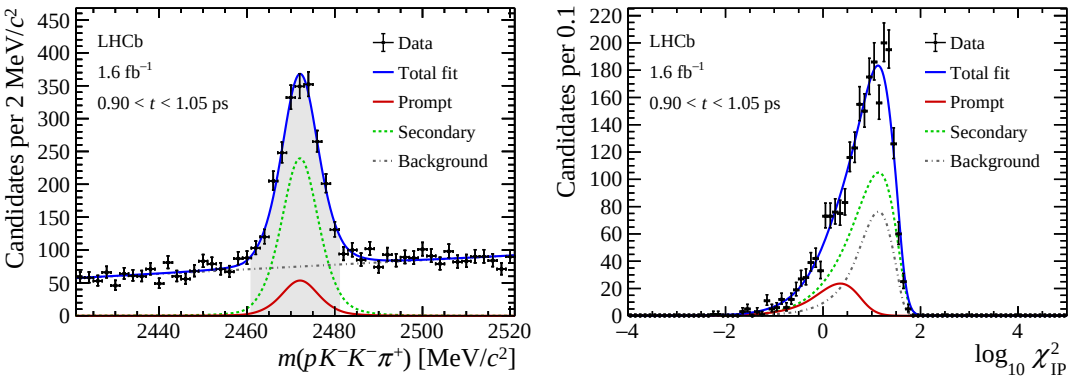

Figure 12: Distributions of (left) invariant mass and (right) $\log_{10}\chi^2_{\rm IP}$ in the reduced mass region of $[2461, 2481]\,\mathrm{MeV}/c^2$ for the Ξ_c^0 data sample collected in 2016 in the decay-time interval of $[0.90, 1.05]\,\mathrm{ps}$, along with the fit results. The contributions of the signal, the secondary decays, and the combinatorial background are shown in red (solid), green (dashed), and gray (dash-dotted), respectively.

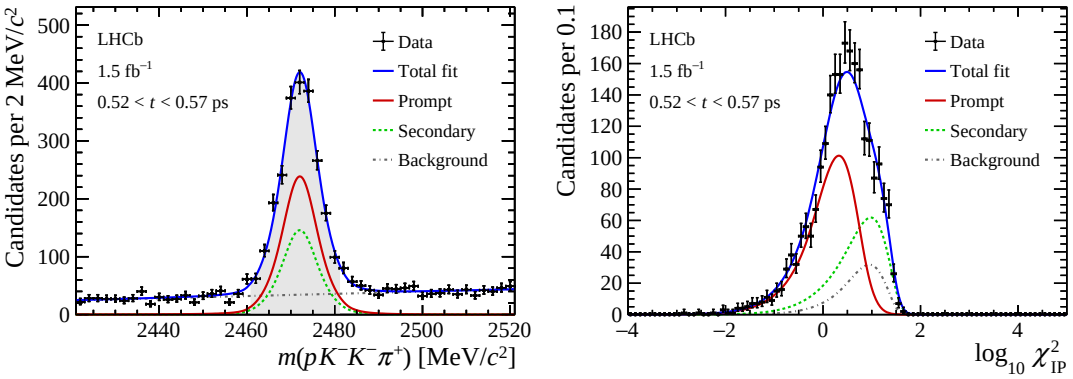

Figure 13: Distributions of (left) invariant mass and (right) $\log_{10}\chi^2_{\rm IP}$ in the reduced mass region of $[2461, 2481]\,\text{MeV}/c^2$ for the Ξ_c^0 data sample collected in 2017 in the decay-time interval of $[0.52, 0.57]\,\text{ps}$, along with the fit results. The contributions of the signal, the secondary decays, and the combinatorial background are shown in red (solid), green (dashed), and gray (dash-dotted), respectively.

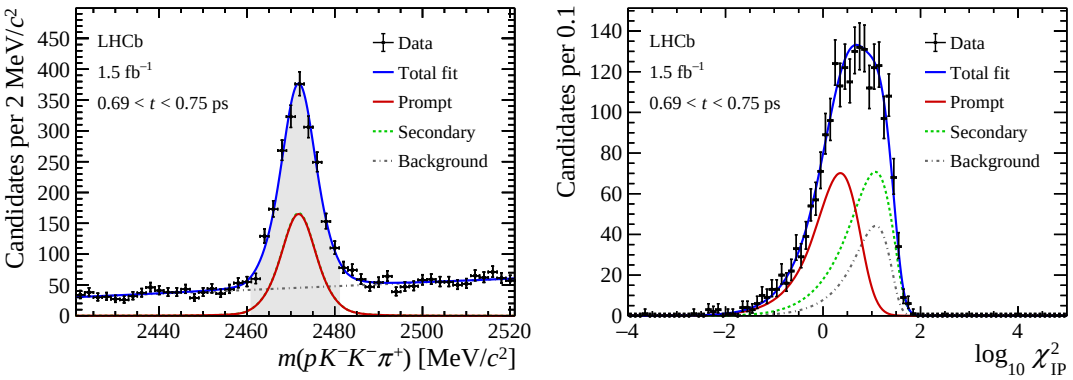

Figure 14: Distributions of (left) invariant mass and (right) $\log_{10}\chi^2_{\rm IP}$ in the reduced mass region of $[2461, 2481]\,\text{MeV}/c^2$ for the Ξ_c^0 data sample collected in 2017 in the decay-time interval of $[0.69, 0.75]\,\text{ps}$, along with the fit results. The contributions of the signal, the secondary decays, and the combinatorial background are shown in red (solid), green (dashed), and gray (dash-dotted), respectively.

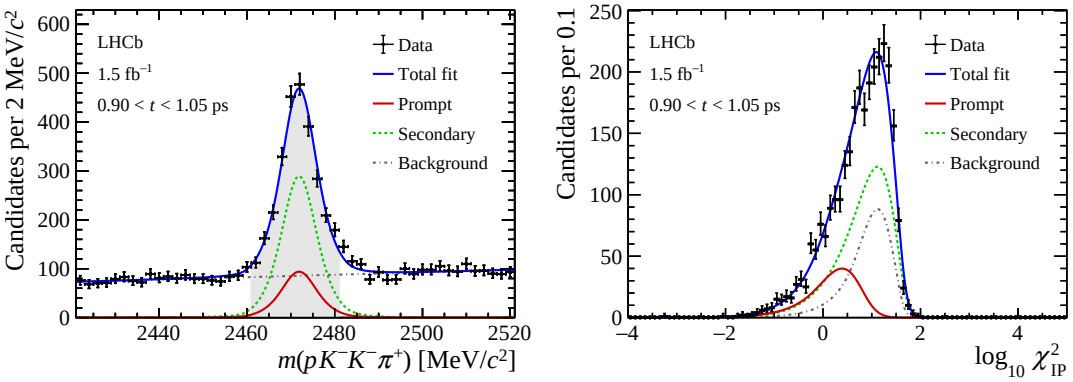

Figure 15: Distributions of (left) invariant mass and (right) $\log_{10}\chi^2_{\rm IP}$ in the reduced mass region of $[2461, 2481]\,\text{MeV}/c^2$ for the Ξ_c^0 data sample collected in 2017 in the decay-time interval of $[0.90, 1.05]\,\text{ps}$, along with the fit results. The contributions of the signal, the secondary decays, and the combinatorial background are shown in red (solid), green (dashed), and gray (dash-dotted), respectively.

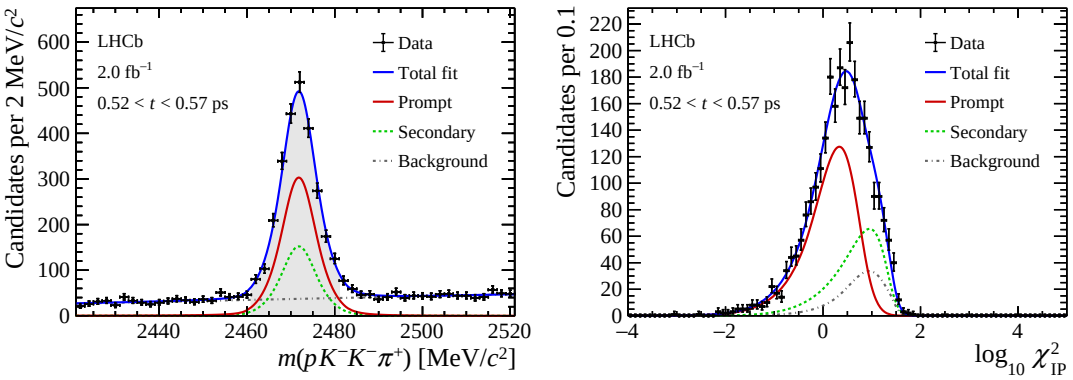

Figure 16: Distributions of (left) invariant mass and (right) $\log_{10}\chi^2_{\rm IP}$ in the reduced mass region of $[2461, 2481]\,\text{MeV}/c^2$ for the Ξ_c^0 data sample collected in 2018 in the decay-time interval of $[0.52, 0.57]\,\text{ps}$, along with the fit results. The contributions of the signal, the secondary decays, and the combinatorial background are shown in red (solid), green (dashed), and gray (dash-dotted), respectively.

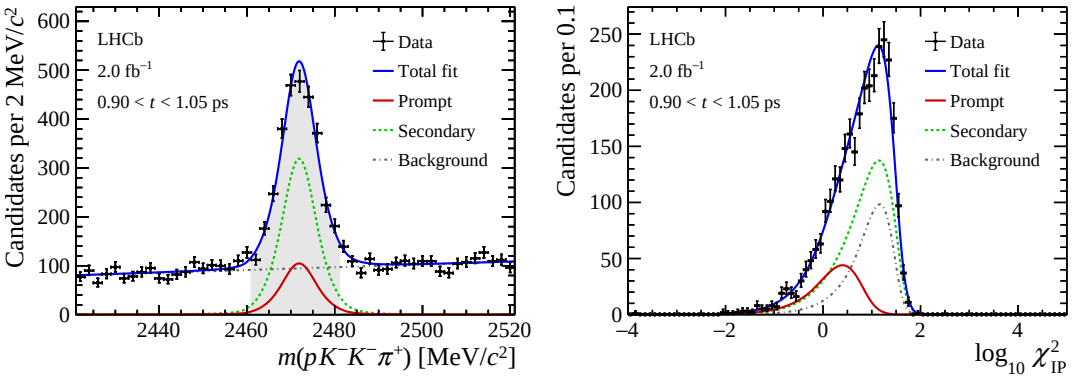

Figure 17: Distributions of (left) invariant mass and (right) $\log_{10}\chi^2_{\rm IP}$ in the reduced mass region of $[2461, 2481]\,\mathrm{MeV}/c^2$ for the Ξ_c^0 data sample collected in 2018 in the decay-time interval of $[0.90, 1.05]\,\mathrm{ps}$, along with the fit results. The contributions of the signal, the secondary decays, and the combinatorial background are shown in red (solid), green (dashed), and gray (dash-dotted), respectively.

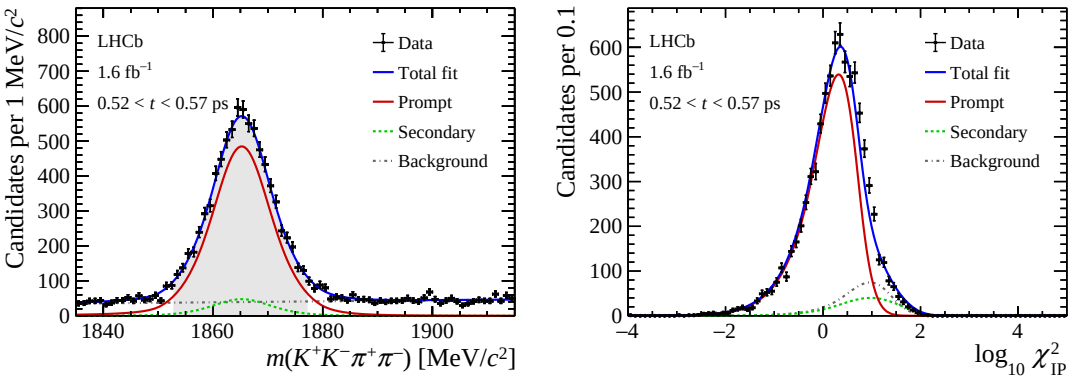

Figure 18: Distributions of (left) invariant mass and (right) $\log_{10}\chi^2_{\rm IP}$ in the reduced mass region of $[1853, 1877]\,\mathrm{MeV}/c^2$ for the D^0 data sample collected in 2016 in the decay-time interval of $[0.52, 0.57]\,\mathrm{ps}$, along with the fit results. The contributions of the signal, the secondary decays, and the combinatorial background are shown in red (solid), green (dashed), and gray (dash-dotted), respectively.

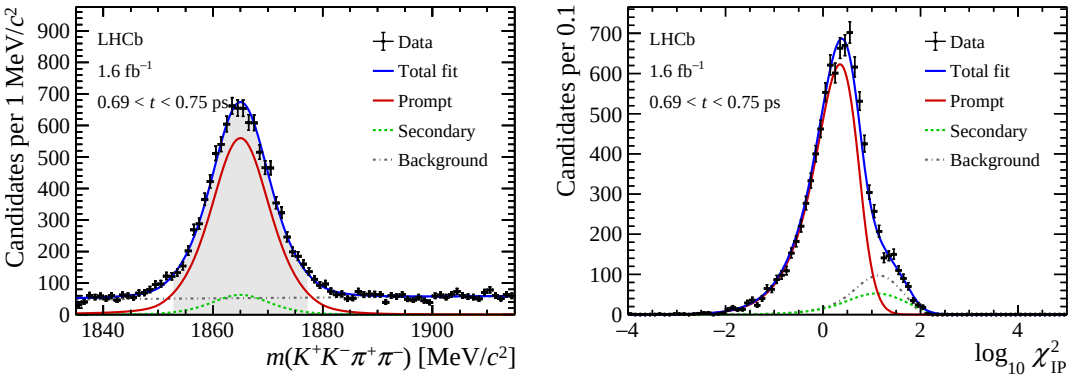

Figure 19: Distributions of (left) invariant mass and (right) $\log_{10}\chi^2_{\rm IP}$ in the reduced mass region of $[1853, 1877]\,\text{MeV}/c^2$ for the D^0 data sample collected in 2016 in the decay-time interval of $[0.69, 0.75]\,\text{ps}$, along with the fit results. The contributions of the signal, the secondary decays, and the combinatorial background are shown in red (solid), green (dashed), and gray (dash-dotted), respectively.

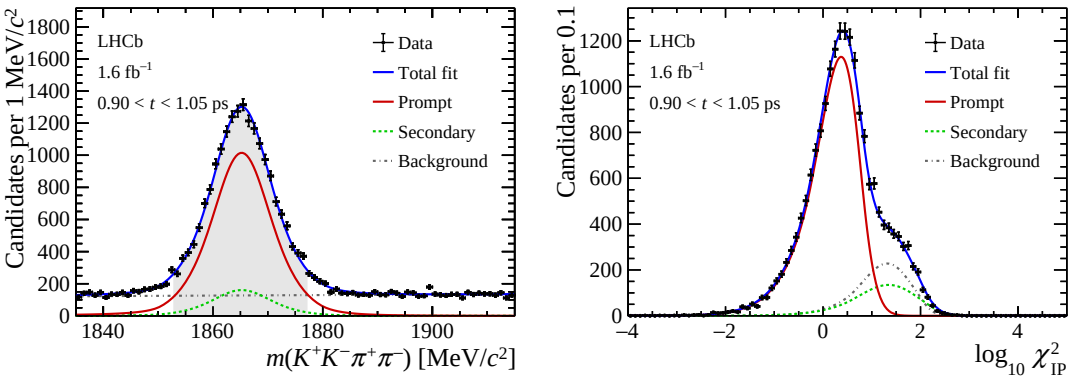

Figure 20: Distributions of (left) invariant mass and (right) $\log_{10}\chi^2_{\rm IP}$ in the reduced mass region of $[1853, 1877]\,\text{MeV}/c^2$ for the D^0 data sample collected in 2016 in the decay-time interval of $[0.90, 1.05]\,\text{ps}$, along with the fit results. The contributions of the signal, the secondary decays, and the combinatorial background are shown in red (solid), green (dashed), and gray (dash-dotted), respectively.

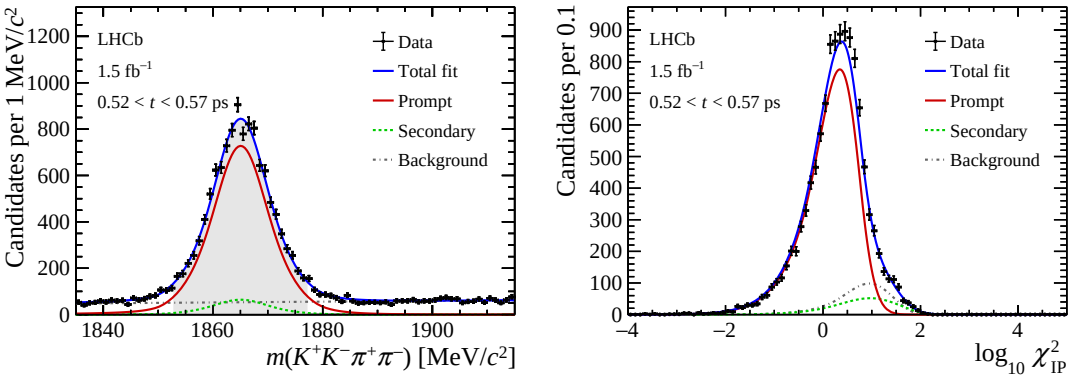

Figure 21: Distributions of (left) invariant mass and (right) $\log_{10}\chi^2_{\rm IP}$ in the reduced mass region of $[1853, 1877]\,\text{MeV}/c^2$ for the D^0 data sample collected in 2017 in the decay-time interval of $[0.52, 0.57]\,\text{ps}$, along with the fit results. The contributions of the signal, the secondary decays, and the combinatorial background are shown in red (solid), green (dashed), and gray (dash-dotted), respectively.

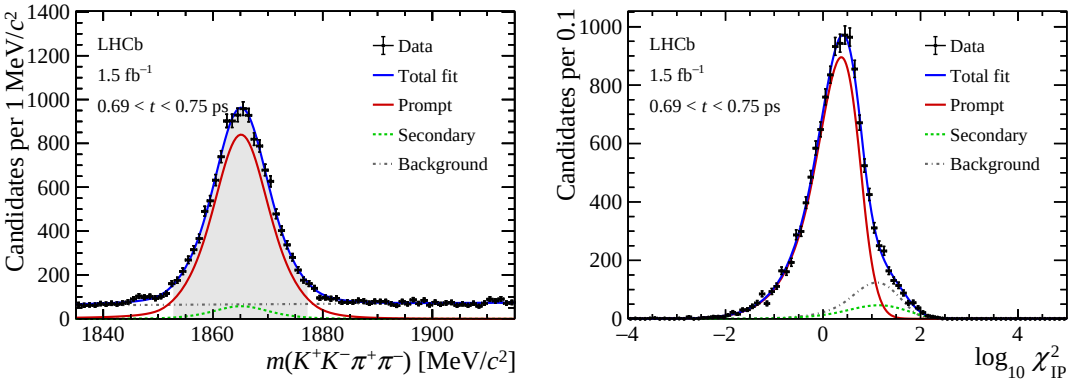

Figure 22: Distributions of (left) invariant mass and (right) $\log_{10}\chi^2_{\rm IP}$ in the reduced mass region of $[1853, 1877]\,\text{MeV}/c^2$ for the D^0 data sample collected in 2017 in the decay-time interval of $[0.69, 0.75]\,\text{ps}$, along with the fit results. The contributions of the signal, the secondary decays, and the combinatorial background are shown in red (solid), green (dashed), and gray (dash-dotted), respectively.

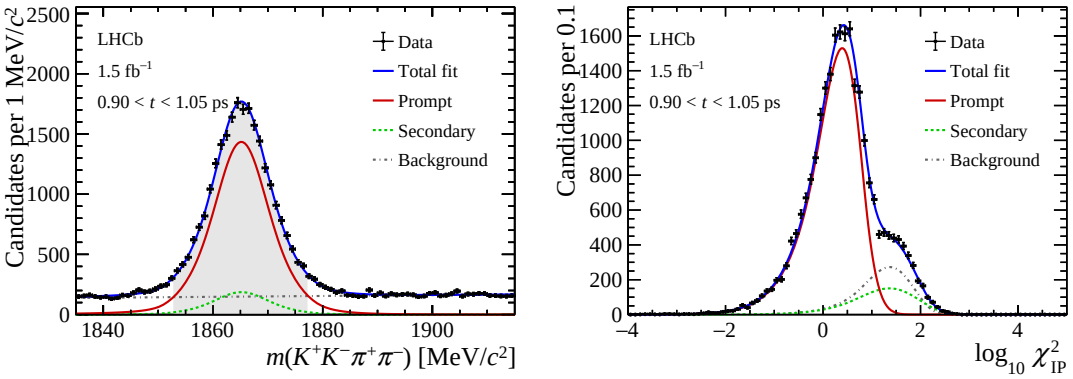

Figure 23: Distributions of (left) invariant mass and (right) $\log_{10}\chi^2_{\rm IP}$ in the reduced mass region of $[1853, 1877]\,\text{MeV}/c^2$ for the D^0 data sample collected in 2017 in the decay-time interval of $[0.90, 1.05]\,\text{ps}$, along with the fit results. The contributions of the signal, the secondary decays, and the combinatorial background are shown in red (solid), green (dashed), and gray (dash-dotted), respectively.

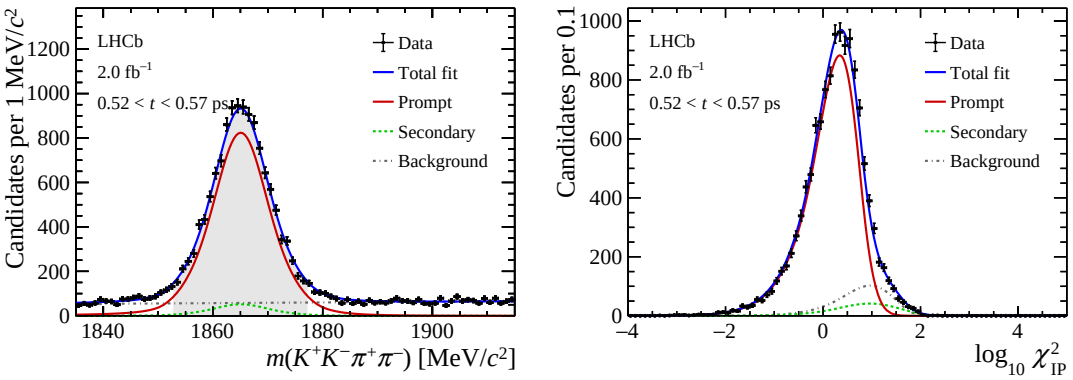

Figure 24: Distributions of (left) invariant mass and (right) $\log_{10}\chi^2_{\rm IP}$ in the reduced mass region of $[1853, 1877]\,\text{MeV}/c^2$ for the D^0 data sample collected in 2018 in the decay-time interval of $[0.52, 0.57]\,\text{ps}$, along with the fit results. The contributions of the signal, the secondary decays, and the combinatorial background are shown in red (solid), green (dashed), and gray (dash-dotted), respectively.

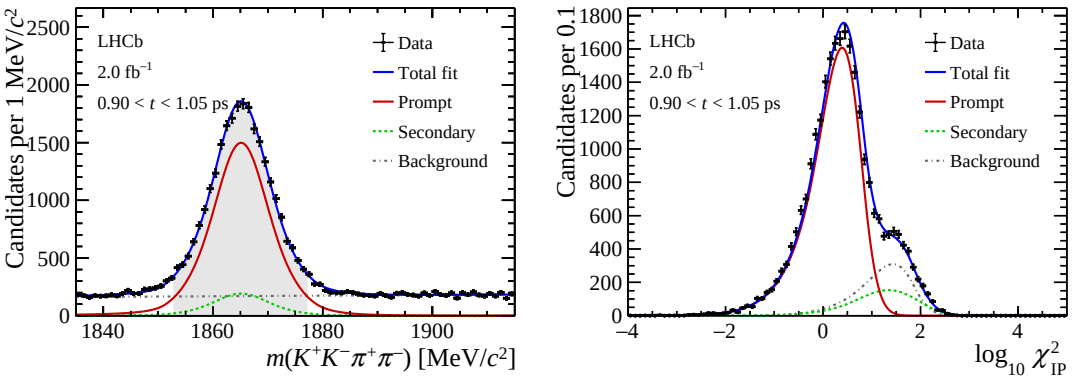

Figure 25: Distributions of (left) invariant mass and (right) $\log_{10}\chi^2_{\rm IP}$ in the reduced mass region of $[1853, 1877]\,\text{MeV}/c^2$ for the D^0 data sample collected in 2018 in the decay-time interval of $[0.90, 1.05]\,\text{ps}$, along with the fit results. The contributions of the signal, the secondary decays, and the combinatorial background are shown in red (solid), green (dashed), and gray (dash-dotted), respectively.

References

[1] LHCb collaboration, R. Aaij *et al.*, *Measurement of the Ω_c^0 lifetime*, Phys. Rev. Lett. **121** (2018) 092003, arXiv:1807.02024.

[2] LHCb collaboration, R. Aaij *et al.*, *Precision measurement of the Λ_c^+, Ξ_c^+, and Ξ_c^0 baryon lifetimes*, Phys. Rev. **D100** (2019) 032001, arXiv:1906.08350.

[3] Particle Data Group, M. Tanabashi *et al.*, *Review of particle physics*, Phys. Rev. **D98** (2018) 030001.